Digital Twin of Vehicle-Track System for Integrated Track Condition Monitoring

Chen Shen(✉), Rolf Dollevoet, and Zili Li

Delft University of Technology, Delft, Netherlands
c.shen-2@tudelft.nl

Abstract. Vibrations resulting from dynamic vehicle-track interactions (VTI) offer valuable insights into track conditions. This paper presents an approach for track condition monitoring by detecting and quantifying multiple track degradations using a digital twin of the VTI system. Unlike existing techniques that focus on a specific degradation type at a single track component, our proposed method provides a generic and integrated framework. By combining a physics-based VTI model with a data-driven model, we dynamically update the digital twin's state based on measured axle-box accelerations (ABA). We introduce a local ABA feature extracted from its spectrogram and demonstrate its effectiveness in distinguishing various degradations at different track positions. The implementation and capability of the proposed approach were demonstrated in a case study conducted on a transition zone of a railway bridge. The simultaneous track stiffness variations in the railpad/fastening and ballast layers were successfully detected, confirming the effectiveness of our approach. The case study also showcases the generality, interpretability, efficiency, and robustness of the proposed approach in identifying concurrent degradation. Our proposed framework opens new possibilities for cost-effective continuous track monitoring for railway infrastructure management.

1 Introduction

Vibrations caused by dynamic vehicle-track interactions (VTI) provide valuable information about track conditions. Hence, measured vibration signals from rail vehicles, such as axle-box accelerations (ABA), can be used as a cost-effective source for continuous track monitoring. Existing ABA techniques are focused on identifying a specific type of degradation, usually at a single track component, such as at the rail top [1], track geometry [2], fastenings [3], ballast and substructures (track stiffness) [4], etc. The basic principle is to identify unique ABA features that correspond to a particular degradation. However, different types of degradation may cause similar changes in specific ABA features. As a result, it is still challenging to distinguish between various types of track degradations, particularly when they occur at different track layers at the same time.

In this paper, instead of focusing on a single type of track degradation, we propose an integrated and generic approach for detecting and quantifying multiple track degradations using a digital twin of the VTI system. The implementation and capability of the proposed digital twin are demonstrated in a case study, where the proposed approach was

W. Huang and M. Ahmadian (Eds.): IAVSD 2023, LNME, pp. 743–751, 2025.
https://doi.org/10.1007/978-3-031-66971-2_77

applied to evaluate the simultaneous track stiffness variations in the railpad/fastening and ballast layers.

2 Digital Twin Framework

Figure 1(a) shows the quantities of interest (QoI) for the physical asset and their counterparts in the digital twin. Track conditions are represented by the physical state S and digital state D. Measured and simulated vibration signals, such as ABA, are represented by observations O and predications P. In practice, vibration signals usually need to be transformed to a feature space X for further analysis.

Two models, i.e., a physics-based VTI model and a data-driven model, are developed to virtually represent the VTI system and define the relationships between the QoI, as shown in Fig. 1(b). In particular, the task is to dynamically update the digital state $\boldsymbol{d} \in D$ using observed ABA feature $\boldsymbol{x^o} \in X$.

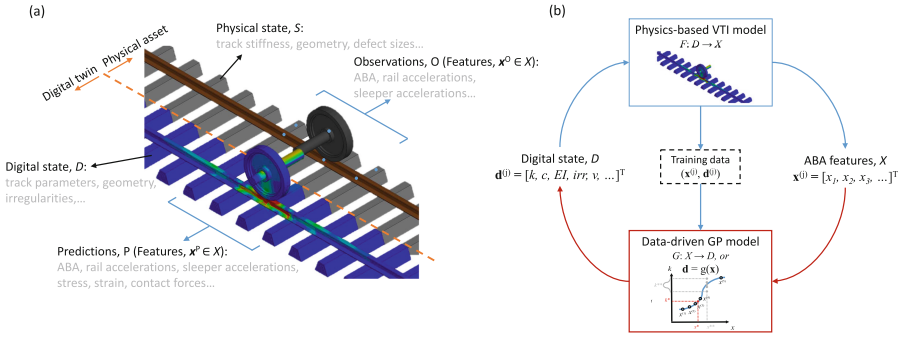

Fig. 1. Digital twin framework for VTI system. (a) Four quantities of interest (QoI) representing the digital twin and its associated physical VTI system. (b) Strategy for dynamically updating the digital state of the digital twin by combining a physics-based VTI model and a data-driven model.

3 Implementation

3.1 ABA Features

Figure 2 shows the spectrograms of for a section of measured ABA signal calculated using the short-time Fourier transform. The changing characteristic frequencies and spectrum power at different track locations can be used as ABA features.

Thus, at each track location d, we propose to use both the characteristic frequencies and spectrum power to construct the feature vector $\boldsymbol{x}^{(d)}$. In particular, a window was first applied to the ABA signal, which was centered at a sleeper position with a length of two sleeper spans. Subsequently, the power spectrum density (PSD) of the windowed ABA signal was calculated. This local PSD was used as the feature vector of ABA. Thus, measured feature vectors at different track locations constitute a measured feature space X.

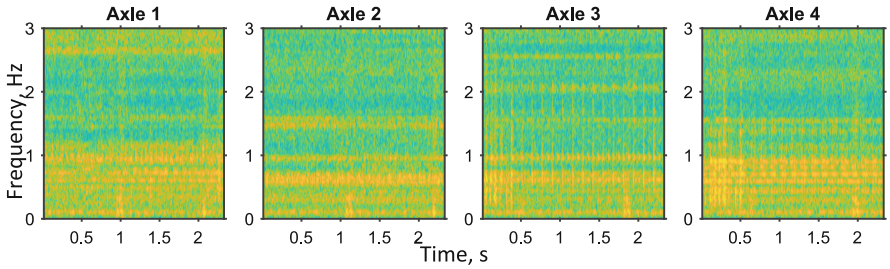

Fig. 2. Spectrograms of the ABAs measured from four axles of a wagon.

3.2 Forward Mapping: From Digital State to ABA Features

A high-dimensional digital state space D is defined to represent track conditions (such as the track geometry and railpad/ballast stiffness) and operational variables (such as the axle load and vehicle speed). The D space covers both the nominal and degraded values for each parameter. We sample from the D space to obtain multiple sets of input parameters $\boldsymbol{d}^{(j)}$ for the VTI model. Each $\boldsymbol{d}^{(j)}$ presents a unique track condition, with different degradation types and severities in different track components. Through simulations with sampled parameters, a data set containing the forward mapping from the digital state space D to the feature space X is generated. The VTI model is then validated by comparing the simulated feature space to the measured one.

3.3 Inverse Mapping: From ABA Features to Track Conditions

Data-driven models can be developed based on the data set to represent the inverse mapping from the feature space to the digital state space. A model selector was employed in this study and it has the advantage of being directly applicable to a model library without the need to train a data model.

The model selector searches directly within the data set for one or several model instances $m_j \sim (\boldsymbol{x}^{(j)}, \boldsymbol{d}^{(j)})$ that best match an observation $\boldsymbol{x}^*$. The model selector establishes can be denoted as.

Thus, we are able to assess the track condition (physical state S) through the lens of the digital state D, given that simulated and measured ABA share the same feature space X, as has been shown in Sect. 3.2. The simulations are time-consuming and performed offline. The monitoring can be carried out online or in near real-time due to the computational efficiency of the GP model.

4 Case Study

We use the proposed digital twin to monitor a track section with fastening and ballast stiffness variations. Field observations and hammer tests are used to validate the monitoring results. We show that the proposed approach is generic, physically interpretable, fast to implement, and robust to concurrent degradations.

4.1 Field Measurements

Field measurements were conducted to validate the proposed approach. The test site was chosen at a railway bridge between Murjek and Boden in the Iron Ore line in Sweden, as shown in Fig. 3. Track stiffness variations from the transition zone to the bridge under 10 sleepers (i.e., sp_1–sp_{10} in Fig. 3) were evaluated using two techniques.

The first technique employs ABA to assess track stiffness, as proposed in this report. An in-service passenger train regularly travelling on the Iron Ore Line was instrumented. Accelerometers were installed on all eight axle boxes of a wagon, measuring in three directions: vertical, longitudinal, and lateral. Only vertical accelerations were used for track stiffness evaluation. ABA data were collected during four passes of the train through the test site, two in the direction of Boden and two in the direction of Murjek.

The second technique is the track structure hammer test method [5], which is used to compare with and validate the track stiffness evaluated by the ABA. Track receptances were measured using hammer tests on the rail top above 10 sleepers (i.e., sp_1–sp_{10} in Fig. 5.3.3-2). The railpad and ballast stiffnesses under the 10 sleepers can then be obtained based on the measured track receptances [5].

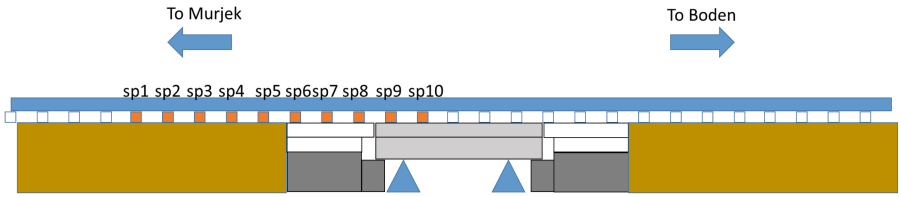

Fig. 3. Schematic of the field measurement site.

4.2 Validation of the VTI Model

The VTI model was validated against the track receptances measured by the hammer test and the PSDs obtained from the ABA measurement at the test site. The purpose was to ensure that the numerical model accurately captures the primary dynamic characteristics of the VTI system. A comprehensive examination of the dynamic characteristics of the VTI system can be found in Appendix 5.3.3-b (some results were also included in the interim report and are not reiterated here).

Figure 4 compares the measured and simulated track recetpances. The track receptances measured at the 10 sleepers are presented, while the simulated receptance using one set of track parameters is shown. Both the measured and simulated track receptances reveal two track resonances [5]:

- The full-track (FT) resonance: where the rail and sleeper vibrate in-phase at rail seats.
- The rail (R) resonance: where the rail vibrates in anti-phase with the sleeper at rail seats.

It can be seen from the measurements that the magnitude of track receptances at different sleepers exhibits larger variations in the frequency range of the FT resonance

(below 80 Hz) compared to the range around the R resonance (150–500 Hz). This suggests that the variations in ballast stiffness are more significant than the variations in railpad stiffness across these 10 sleepers [5].

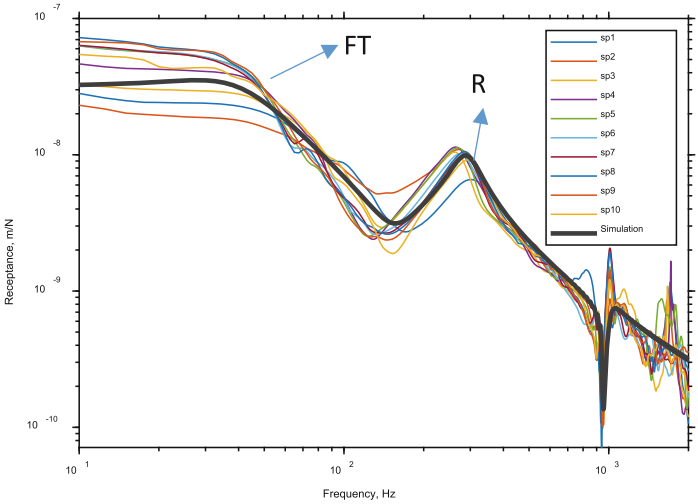

Fig. 4. Comparison of measured and simulated track receptances.

Figure 5 compare the PSDs obtained from the ABA measured from different axle boxes. Each subplot shows the ABA measurement from a specific axle box. Within each subplot, the measured local PSDs (as defined in the Sect. 3.1) at the 10 sleepers are shown by the red lines. The simulated PSDs of the ABA measured from the eight axle boxes of the instrumented wagon were also presented.

The measured PSDs exhibit variations across different axles, at various sleepers, and in different directions. However, the major frequency peaks align well with the resonances predicted by the VTI model. These peaks correspond to the following resonances of the VTI system:

- The full-track (FT) resonance: where the wheel and track vibrate together on the track support stiffness.
- The sleeper-anti (SA) resonance: where the sleeper vibrates in between the rail and ballast.
- The rail-bending-between-wheelsets (RBW) resonance: where the rail vibrates at different wavelengths between the two wheels in a bogie (in the longitudinal direction).

4.3 Track Stiffness Evaluation

The railpad and ballast stiffness across the 10 sleepers were evaluated using both the ABA measurement and hammer test.

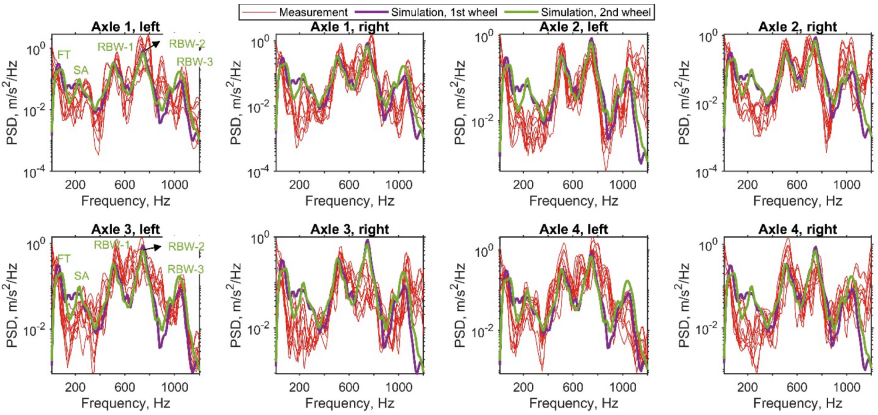

Fig. 5. Comparison of measured and simulated PSD of ABA (running direction: from Murjek to Boden).

Figure 6 show the results for the evaluation of railpad stiffness. Based on the sensitivity analysis [5, 6], the track receptance (150–800 Hz) obtained from the hammer test and the local PSD (150–1200 Hz) obtained from the ABA measurement were used as features for the model selector.

For the evaluation based on the hammer test, the best match from the model library was selected for the track receptance obtained at each sleeper, and the corresponding railpad stiffness was plotted (blue line with triangle markers). The railpad stiffness exhibited a decreasing trend from sp1 to sp5, followed by an increasing trend from sp5 to sp10. A local peak was observed at sp7. Notably, the variations in railpad stiffness evaluated by the hammer tests were relatively small, ranging between approximately 80 MN/m and 140 MN/m, with a median value of approximately 100 MN/m.

Considering that ABA measurements are more susceptible to noise compared to hammer tests, the top ten matches from the model library were plotted for the railpad stiffness evaluated by the ABA. The results were presented in the form of median values (red line) and envelopes (black dashed). In general, the railpad stiffness evaluated by the ABA exhibited a similar trend to the hammer test results, albeit with variations observed across different axles (Fig. 6(a)). However, the median values of the railpad stiffness distributions obtained from the ABA measurements at different axle boxes ranged between 200 MN/m and 300 MN/m, approximately 2 to 3 times higher than the values evaluated by the hammer tests (Fig. 6(b)). This difference can be attributed to the fact that the ABA measures track stiffness under loaded conditions, while the hammer test measures unloaded track stiffness. Furthermore, the stiffness variations across the 10 sleepers (approximately 100–500 MN), including the local change at sp7, were more pronounced in the ABA measurements compared to the hammer tests, possibly due to the significant dynamic effects induced by train-track interaction, amplifying the observed stiffness variations.

Figure 7 presents the results for the evaluation of ballast stiffness with different train running directions. The track receptance and local PSD in the frequency range of 20–150 Hz were used as features for the model selector.

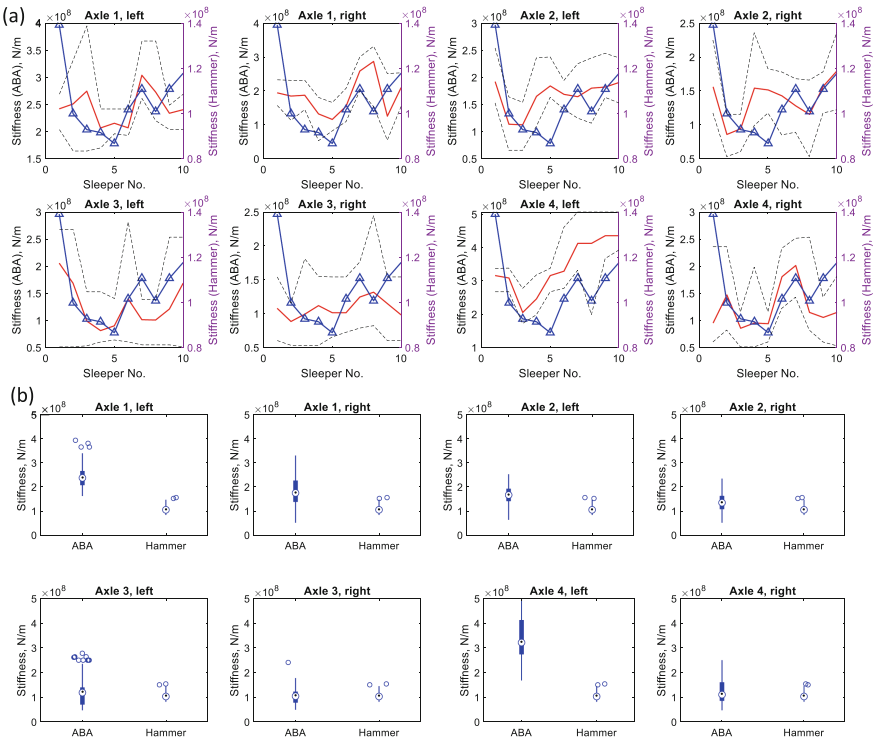

Fig. 6. Comparison of railpad stiffness evaluated by ABA (direction: Murjek to Boden) and hammer test. (a) Variations of railpad stiffness across 10 sleepers (sp_1–sp_{10} in Fig. 3). (b) Distributions of railpad stiffness across 10 sleepers.

Based on the results obtained from the hammer tests, the ballast stiffness in the transition zone reaches its maximum at sp2 (40 MN/m) and then gradually decreases towards the bridge, reaching its minimum value of 12 MN/m at sp5. This suggests that the sleepers near the bridge receive less support from the ballast. Between sp5 and sp9, the ballast stiffness remains relatively constant at its minimum value and then increases further to 27 MN/m at sp10. This variation in ballast stiffness may reflect the support conditions of the bridge. As depicted in Fig. 3, the support of the north abutment to the bridge has degraded over time, resulting in the installation of a new steel I-beam under sp9 and sp10 to bear the support of the bridge. Consequently, a sudden increase in ballast stiffness was observed at these locations.

In terms of the ABA evaluations, the ballast stiffness differs among the axle boxes. The axle boxes on the left side exhibit better ballast stiffness evaluations that align with the variation pattern indicated by the hammer tests, compared to those on the right side for both running directions. Similar to the evaluations of railpad stiffness, the median values and variations of ballast stiffness across the 10 sleepers, as evaluated by the ABA, are larger than those obtained from the hammer tests. This can be attributed to the loaded condition and the dynamic amplification effect in the ABA measurements. Furthermore,

for the ABA results, the median values and variations of ballast stiffness are larger when the train runs from the bridge to the transition zone (from Boden to Murjek).

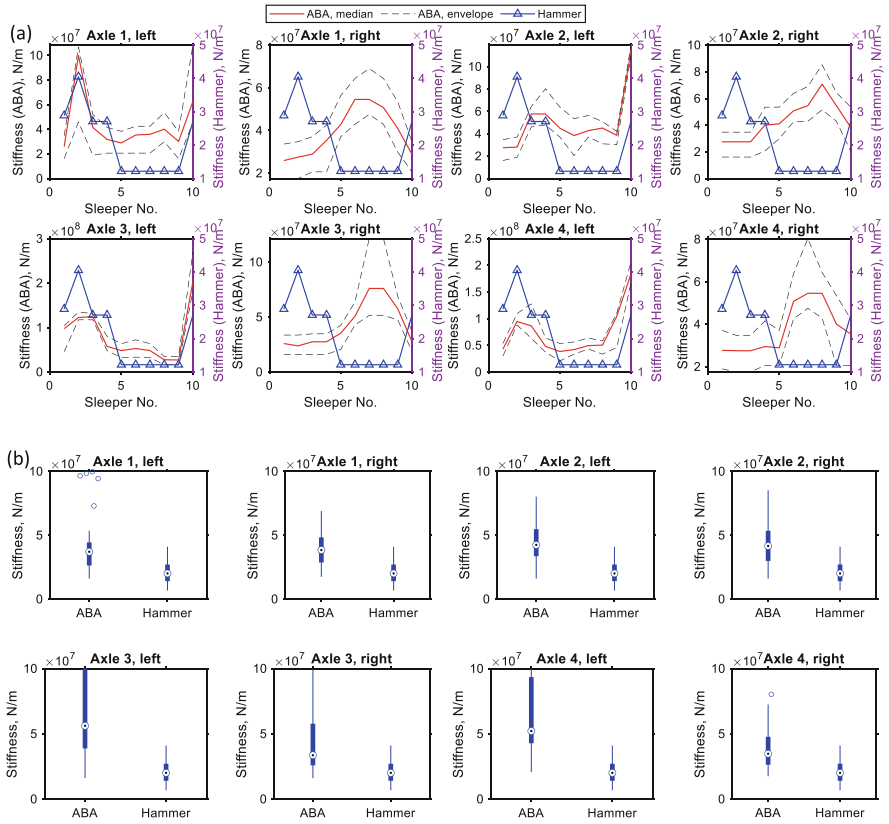

Fig. 7. Comparison of ballast stiffness evaluated by ABA (direction: Murjek to Boden) and hammer test. (a) Variations of railpad stiffness across 10 sleepers (sp1–sp10 in Fig. 3). (b) Distributions of railpad stiffness across 10 sleepers.

5 Conclusion

In this study, we presented an integrated digital twin approach for detecting and quantifying multiple track degradations in vehicle-track interactions (VTI). By leveraging the capabilities of a digital twin, we proposed a generic framework that goes beyond single-component degradation detection. Our approach combines a physics-based VTI model with a data-driven model selector, allowing for dynamic updates of the digital twin's state based on measured axle-box accelerations (ABA).

By considering both characteristic frequencies and spectrum power of windowed ABA signal, we constructed a local feature vector that enabled accurate positioning of

degradation occurring at different track layers simultaneously. This approach addresses the limitations of existing techniques that focus on a single type of degradation at a specific track component.

Field validation experiments conducted on a railway bridge demonstrated the practical applicability of our proposed approach. The results confirmed that our digital twin framework provides accurate and interpretable assessments of track conditions, making it a valuable tool for continuous track monitoring and maintenance planning.

References

1. Molodova, M., Li, Z.L., Nunez, A., Dollevoet, R.: Automatic detection of squats in railway infrastructure. IEEE Trans. Intell. Transp. Syst. **15**, 1980–1990 (2014)
2. De Rosa, A., Alfi, S., Bruni, S.: Estimation of lateral and cross alignment in a railway track based on vehicle dynamics measurements. Mech. Syst. Signal Process. **116**, 606–623 (2019). https://doi.org/10.1016/J.YMSSP.2018.06.041
3. Chen, M., Zhai, W., Zhu, S., Xu, L., Sun, Y.: Vibration-based damage detection of rail fastener using fully convolutional networks. **60**, 2191–2210 (2021). https://doi.org/10.1080/00423114.2021.1896010
4. Berggren, E.G., Kaynia, A.M., Dehlbom, B.: Identification of substructure properties of railway tracks by dynamic stiffness measurements and simulations. J. Sound Vib. **329**, 3999–4016 (2010). https://doi.org/10.1016/J.JSV.2010.04.015
5. Shen, C., Dollevoet, R., Li, Z.: Fast and robust identification of railway track stiffness from simple field measurement. Mech. Syst. Signal Process. **152**, 107431 (2021). https://doi.org/10.1016/j.ymssp.2020.107431
6. Shen, C., Zhang, P., Dollevoet, R., Zoeteman, A., Li, Z.: Evaluating railway track stiffness using axle box accelerations: a digital twin approach. Mech. Syst. Signal Process. **204**, 110730 (2023). https://doi.org/10.1016/j.ymssp.2023.110730